第八届（2003 年）全国空气弹性学术交流会论文

NS 方法数值预测跨音速气动颤振边界

杨国伟

（中国科学院力学研究所，北京，10080）

摘　要　本文通过耦合求解三维薄层 Navier-Stokes 方程与结构运动方程数值模拟了跨音速气动颤振现象。其中，流动控制方程的求解采用具有三阶精度的 HLLEW(Harten-Lax-van Leer-Einfeldt Wada) 迎风 TVD 空间离散格式和 LU-SGS 内迭代时间推进方法，同样的内迭代方法用于结构运动方程的求解。在每一步实时推进计算中，通过内迭代，使整个耦合计算的时间精度达到二阶。针对每一时间步的结构变形，发展了一种自适应网格变形方法，在中等结构变形的情况下，该方法能保证变形后的网格具有原网格的质量。为检验发展的跨音速气动颤振计算程序，对一标准气动弹性机翼的跨音速气动弹性边界进行了计算，获得了与实验一致的结果。另外，还详细研究了网格数、时间步长及内迭代步数对气动颤振计算的影响。

关键词　Navier-Stokes 方程；数值模拟；跨音速；气动颤振

1 Introduction

In recent years, dynamic aeroelastic simulations by solving three-dimensional Navier-Stokes equations coupled with structural equations of motion have been extensively studied [1-3]. However, in these methods, the flow governing equations are only loosely coupled with structural equations, namely, after the aerodynamic loads are determined by solving the flow governing equations, the structural model is used to update the position of body. The coupling contains the error of one time step, thus these methods are always only first-order accuracy in time regardless of the temporal accuracy of the individual solvers of the flow and structural equations. In addition, due to the deformation of aeroelastic configuration, adaptive dynamic grids need to be generated at each time step. In the existing aeroelastic methods, various adaptive algebraic grid-generation methods were applied for their applications.

In the paper, a cell-center finite volume code is implemented for the aeroelastic calculation. The LU-SGS subiteration algorithm is constructed for the thin-layer Navier-Stokes equations, and the modified Harten-Lax-van Leer Einfeldt (HLLE) scheme [3] is used for the discretization of convective terms of the flow governing equations. The structural equations of motion in generalized coordinates are employed for the calculation of structures. A grid deformation approach suitable for the moderate aeroelastic deformation is also developed.

The AGARD445.6 standard aeroelastic wing test case [4] is applied to validate the resulting aeroelastic solver. The aeroelastic boundaries are calculated from subsonic to supersonic flow. The effects of grid resolution, time-step sizes are also discussed.

2 Governing Equations

2.1 Aerodynamic Governing Equations

Aerodynamic governing equations are the unsteady, three-dimensional thin-layer Navier-Stokes equations in strong conservation law form, which can be written in curvilinear coordinates as

$$\partial_t \hat{Q} + \partial_\xi F + \partial_\eta G + \partial_\zeta H = \partial_\zeta H_v + S_{GCL} \qquad (1)$$

The source term S_{GCL} is obtained from the geometric conservation law for moving mesh, which is defined as

$$S_{GCL} = Q\left[\partial_t J^{-1} + (\xi_t / J)_\xi + (\eta_t / J)_\eta + (\zeta_t / J)_\zeta\right] \qquad (2)$$

2.2 Structural dynamic Governing Equations

Second-order linear structural dynamic governing equations after normalized similar to the flow governing equation can be written as

$$[M]\{\ddot{d}\} + [K]\{d\} = \{F\} \qquad (3)$$

With these first N modes we have an approximate description of the displacement vector of the system can be given by $\{d\} = [\Phi]\{q\}$. Since the natural modes are orthogonal with respect to both the mass and stiffness matrices, premultiplying Equation 3 by $[\Phi]^T$ yields structural equations in generalized coordinates

$$\ddot{q}_i + 2\zeta_i \omega_i \dot{q}_i + \omega_i^2 q_i = [\Phi]_i^T F / M_i \qquad (4)$$

where $\omega_i^2 = [\Phi]_i^T \{K\}[\Phi]$, $M_i = [\Phi]_i^T \{M\}[\Phi]$

The modal damping is readily added on the left hand side of Equation 4, where ζ_i is the damping ratio in the i th mode.

3 Numerical Method

LU-SGS method, employing a Newton-like subiteration, is used for solving Equation 1. Second-order temporal accuracy is obtained by utilizing three-point backward difference in the subiteration procedure. The inviscid terms are approximated by modified third-order upwind HLLE scheme [3]. For the isentropic flow, the scheme results in the standard upwind-biased flux-difference splitting scheme of Roe, and as the jump in entropy becomes large in the flow, the scheme turns into the standard HLLE scheme. Thin-layer viscous term in Equation 1 is discretized by second-order

central difference.

The subiteration method can also be applied to the structural equations of motion in generalized coordinates of Equation 4. The resulting scheme is

$$\begin{bmatrix} 1 & -\phi^i \Delta t \\ \phi^i \Delta t \omega_i^2 & 1+2\phi^i \omega_i \zeta_i \Delta t \end{bmatrix} \Delta S = -\phi^i \{(1+\phi) S^p - (1+2\phi) S^n + \phi S^{n-1} + \Delta t \begin{bmatrix} 0 & -1 \\ \omega_i^2 & 2\omega_i \zeta_i \end{bmatrix} S^p - \Delta t \begin{bmatrix} 0 \\ [\Phi]_i^T F^p / M_i \end{bmatrix} \} \tag{5}$$

where $S = [q, \dot{q}]$ and $\Delta S = S^{p+1} - S^p$. As $p \to \infty$, a full implicit second-order temporal accuracy scheme is formed by the coupling solutions of flow and structural equations. Numerical experiments indicate the calculated results are nearly unchangeable as $p \geq 3$. In the following calculation, the number of subiteration is set to 3.

4 Grid Deformation Method

For the aeroelastic application, if the grid is regenerated at every time step, then the elaborate and time-consuming grid-generation method cannot be used. So in most common aeroelastic sovlers, only algebraic grid generation methods are employed. Recently, a grid deformation method was developed for the aeroelastic calculation by Melville et al [5]. The initial grid of high quality can be generated with any elaborate grid-generation method. The adaptive grid at each time step is obtained by an algebraic grid deformation approach and the grid maintains nearly the same quality of the initial mesh.

First a reference grid $r_{i,j,k}$ is constructed from the initial grid $x_{i,j,k}$ and the deformed surface grid point $x'_{i,j,1}$ was calculated from the structural equations.

$$r_{i,j,k} = x_{i,j,1} + \Delta x_{i,j,1} + [R](x_{i,j,k} - x_{i,j,1}) \tag{6}$$

where $\Delta x_{i,j,1} = x'_{i,j,1} - x_{i,j,1}$ is the deformed size of the surface grid and $[R]$ is the surface rotation matrix defined by unit normal vectors of the original surface and the perturbed surface. The new dynamic grid can be generated by applying a blending function to the reference and the original grids:

$$x'_{i,j,k} = b_{i,j,k} x_{i,j,k} + (1 - b_{i,j,k}) r_{i,j,k} \tag{7}$$

A blending choice is a cubic function in arc-length space with zero slope at the endpoints, which maintains the wall grid orthogonality and smoothly transitions in the far field. This can be written as

$$b_{i,j,k} = 3(s_{i,j,k} / s_{i,j,k_{\max}})^2 - 2(s_{i,j,k} / s_{i,j,k_{\max}})^3 \tag{8}$$

where $k_{\max}$ is the last node in the grid normal direction. The arc-length $s_{i,j,k}$ can be calculated by

$$s_{i,j,k} = \sum_{l=2}^{k} \left| x_{i,j,l} - x_{i,j,l-1} \right| \qquad (9)$$

5 Results and Discussion

The AGARD 445.6 weakened wing model [4] is considered, which has an aspect ratio 1.6525, a taper ratio of 0.6576, a quarter-chord swept angle of 45 deg and a NACA 65A004 airfoil section. A C-H type grid is used. For the baseline grid of $161\times51\times43$, there are 121 grid points around the wing surface, and 39 grid points on the spanwise direction of wing surface. For the refined grid of $181\times51\times63$, 20 grid points are added both in the chord and normal directions.

The first four structural modes and natural frequencies provided in the reference [4] are used for the present computation. To match the given mode shapes to the corresponding aerodynamic surface grid, linear and spline interpolations are employed in the chord and spanwise directions. Structural damping coefficient is set to zero in the whole calculations. Each Mach number is run for several dynamic pressures to determine the flutter point. As the dynamic pressure is varied, the freestream density and Mach number are held fixed and Reynolds number is allowed to vary. A non-dimensional time step $\Delta t = 0.05$ is used for the flutter computations unless stated. All simulations are started from its corresponding steady flow. At $t = 0$, a small initial velocity perturbation 0.0001 for the first bending mode is applied to the wing.

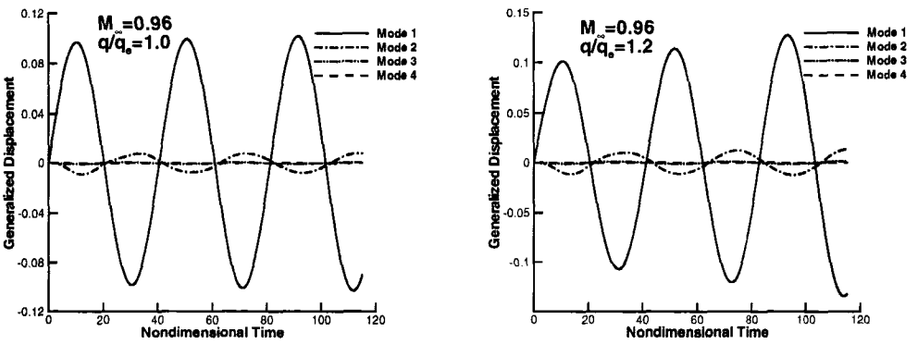

Fig. 1 Dynamic response of first four modes: $M_\infty = 0.96$, $q/q_e = 1.0$ **and** 1.2

The response of the first four modes on the baseline mesh for dynamic pressure $q/q_e = 1.0$ and 1.2 is shown in Fig. 1, where the experimental dynamic pressure for flutter is $q_e = 61.3$ lbf/ft^2. The dominant mode appears to be the first bending mode, and only second mode has some effects to the first mode. The amplification factor of first bending mode is analyzed, which is defined as the ratio of the magnitude of a peak with the magnitude of the previous peak of the same sign. Its corresponding response frequency is determined from the period between these two peaks. For the present case, the

amplification factor and response frequency calculated from the average of the values for the last positive and negative peaks are $AF = 1.023$ and $\omega = 84.135$ rad/sec for $q/q_e = 1.0$ and the corresponding amplification factor and frequency are $AF = 1.093$ and $\omega = 89.559$ rad/sec for $q/q_e = 1.2$. Based on the results of the above two calculations, the dynamic pressure and frequency for flutter ($AF = 1.0$) can be interpolated linearly as $q/q_e = 0.934$, $\omega = 82.353$ rad/sec.

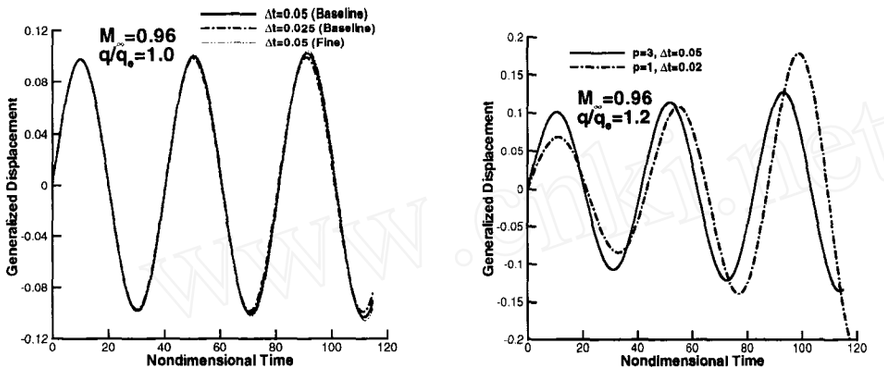

Fig. 2 Effect of grid, time-step sizes, subiteration on mode 1 response

The effect of the size of time step and grid resolution on the response of the first bending mode for $q/q_e = 1$ is demonstrated in Fig. 2. There are only small differences between them. To compromise the computational efficiency and accuracy, the choice of time step and grid is appropriate for the present case. It is seen the reduction of time step leads to a slightly reduction of amplification factor and finer grid grows slightly the oscillation. This indicates that the effect of small time-step size is to reduce the computed flutter speed, but the effect of improved mesh resolution is to increase the speed. The computational efficiency of the full implicit method ($p = 3, \Delta t = 0.05$) is also evaluated by the comparison with the method in which subiteration is not used ($p = 1$) and structural equations of motion are solved using the standard four-stage Runge-Kutta scheme. To ensure the approximate equal total time consuming of the two methods, the time step ($\Delta t = 0.02$) is used for the loosely coupled method. The comparison of the response of mode 1 with the two methods is shown in Fig. 2. The loosely coupled method has significantly enhanced the growth ratio of the oscillation. Based on the influence study of time-step sizes, it indicates the corresponding results can be obtained only for much small time-step size. Namely, the present full implicit coupling method has higher computational efficiency under the same requirements of accuracy and time cost.

Using the method aforementioned, the flutter boundary and frequency are calculated and compared with the experimental data from subsonic 0.338 to supersonic Mach numbers 1.141 in Fig. 3 The

calculated results agree very well the experimental data in the subsonic and transonic range, but are higher than experimental values in the supersonic range.

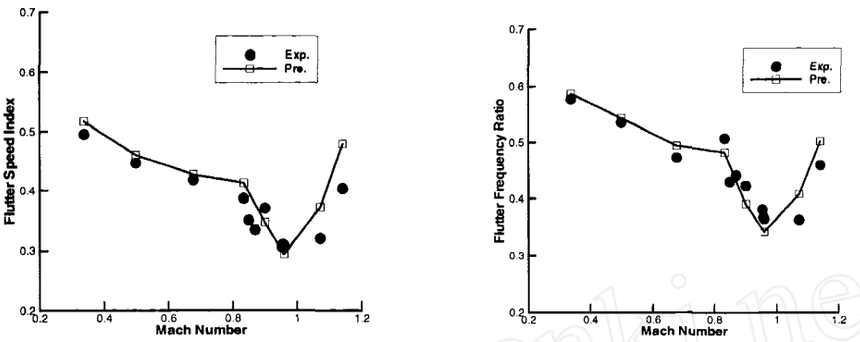

Fig. 3 Flutter speed and frequency for the AGARD 445.6 wing

6. Concluding Remarks

A full implicit finite volume aeroelastic solver has been developed for transonic flutter simulation through the coupled subiteration of the Navier-Stokes equations and structural equations of motion. Results are presented for the AGARD 445.6 standard aeroelastic wing configuration. For subsonic cases, the prediction of the flutter point agrees well with experimental data and simulations previously reported. For the supersonic cases, the present calculation overpredicts the experimental flutter point, but the computed results are better than those of the previous computational results.

References

[1] G. P. Guruswamy: Vortical Flow Computations on Swept Flexible Wings Using Navier-Stokes Equations, AIAA Journal, Vo. 28, 1990, pp.2077-2084.

[2] E. M. Lee-Rausch and J. T. Batina: Wing Flutter Computations Using an Aeroelastic Model Based on the Navier-Stokes, *J. of Aircraft*, Vol.33 1996, pp.1139-1147.

[3] S. Obayashi and G. P. Guruswamy: Convergence Acceleration of a Navier-Stokes Solver for Efficient Static Aeroelastic, AIAA Journal, Vol.33, 1995, pp.1134-1141.

[4] E. C. Jr. Yates: AGARD Standard Aeroelastic Configurations for Dynamic Response I-Wing 445.6, AGARD-R-765, 1988.

[5] R. E. Gordiner and R. B. Melville: Transonic Flutter Simulations Using an Implicit Aeroelastic Solver, J. of Aircraft, Vol.37, 2000, pp.872-879.